$Hf_{0.5}Zr_{0.5}O_2$-Based Ferroelectric Gate HEMTs With Large Threshold Voltage Tuning Range

Chunlei Wu, *Member, IEEE*, Hansheng Ye, *Student Member, IEEE*, Nikhita Shaju, *Student Member, IEEE*, Jeffrey Smith, *Student Member, IEEE*, Benjamin Grisafe, *Student Member, IEEE*, Suman Datta, *Fellow, IEEE*, and Patrick Fay, *Fellow, IEEE*

***Abstract*— AlGaN/GaN high-electron-mobility transistors (HEMTs) with $Hr_{0.5}$ $Zr_{0.5}O_2$ ferroelectric gate stacks exhibiting significant ferroelectric switching for threshold voltage control are experimentally demonstrated. Ferroelectric gate HEMTs (FeHEMTs) with large threshold voltage tuning range of 2.8 V were obtained, with an on/off ratio of $\sim 10^5$ based on a GaN-channel HEMT structure suitable for RF applications. Improved subthreshold performance has also been achieved compared to conventional MIS-HEMTs, with reduction in average sub-threshold swing (SS_{avg}) by a factor of 2. As a consequence of the significant ferroelectric polarization achieved on AlGaN/GaN heterostructures, $Hr_{0.5}$ $Zr_{0.5}O_2$ based ferroelectric gate AlGaN/GaN HEMTs appear promising for nonvolatile and reconfigurable RF and microwave applications.**

***Index Terms*— AlGaN/GaN, $Hr_{0.5}$ $Zr_{0.5}O_2$ (HZO), ferroelectric gate, high-electron-mobility transistors (HEMTs).**

I. Introduction

FERROELECTRIC (FE) devices have attracted much attention for their potential application to a wide range of uses, including memory, steep slope transistors, and neuromorphic computing [1]–[3]. Extensive research has been devoted to FE devices on silicon, including evaluation of ferroelectric devices for possible low-voltage performance optimization and nonvolatile memory applications [4]–[6]. However, an area of particular interest and potential impact is the combination of ferroelectric materials with III-nitrides; the strong polarization of nitrides [7] along with the switchable polarization nature of ferroelectrics [8], [9] can be used to augment polarization engineering for 2D-electron gas (2DEG) channel modulation and dynamic threshold voltage control, opening up potential for multifunctional semiconductor devices for nonvolatile and reconfigurable RF/microwave applications [10]–[12]. For nonvolatile reconfigurable RF switch applications, a large threshold voltage tuning range is needed to retain the switch states in the presence of large RF signal swings, as well as to enhance linearity performance. Prior reports of devices with FE gate stacks on GaN-based HEMTs have focused on achieving enhancement-mode operation or steeper subthreshold performance [13]–[17]. However, the ferroelectric gate HEMTs reported to date exhibit only modest positive threshold voltage shifts and indistinct ferroelectric switching response, which are not suitable for dynamic threshold voltage control in RF applications.

In this work, $Hf_{0.5}Zr_{0.5}O_2$(HZO) based ferroelectric gate HEMTs (FeHEMTs) on AlGaN/GaN heterostructures have been experimentally demonstrated. Due to the high-quality HZO ferroelectric film and dielectric/semiconductor interface achieved, distinct counterclockwise FE hysteresis has been observed in the measured FeHEMTs transfer characteristics. A large threshold voltage tuning range (ΔV_{th}) of 2.8 V has been achieved. In addition, the role of the FE polarization switching of the HZO ferroelectric in the device performance has been evaluated. The results provide insights into routes for exploitation of FE gate stacks on GaN and related materials for nonvolatile RF and microwave applications.

II. Device Fabrication

The schematic cross section of the $Hf_{0.5}Zr_{0.5}O_2$ (HZO) ferroelectric gate HEMT (FeHEMT) based on AlGaN/GaN heterostructure is shown in Fig. 1(a). The epitaxial layers are a conventional MOCVD-grown AlGaN/GaN RF HEMT, consisting of (from the surface) 20 nm $Al_{0.24}Ga_{0.76}N$, 400 nm undoped GaN, and 2 μm GaN buffer layer, on a SiC substrate. The key device fabrication steps are shown in Fig. 1(b). After alignment mark definition, device fabrication started from mesa isolation dry etching using inductively coupled plasma reactive ion etching (ICP-RIE) to a depth of 140 nm, followed by source/drain ohmic contact formation using a Ti/Al/Ni/Au metal stack, annealed at 850°C for 30s in N_2 ambient. Ferroelectric gate stacks consisting of either 2 nm or 4 nm of Al_2O_3 and 10 nm of HZO were grown by atomic layer deposition (ALD) at 250°C. As an experimental control, conventional metal-insulator-semiconductor HEMTs (MIS- HEMTs) with 4 nm Al_2O_3 gate oxide (no HZO) were also fabricated. Gates were formed by sputtering and lift-off of 100 nm of W. A gate stack anneal at 500°C for 30 s in N_2 was performed for

Manuscript received December 28, 2019; revised January 6, 2020; accepted January 7, 2020. Date of publication January 9, 2020; date of current version February 25, 2020. This work was supported in part by the Applications and Systems Driven Center for Energy-Efficient Integrated NanoTechnologies (ASCENT), one of six centers in the Joint University Microelectronics Program (JUMP), Semiconductor Research Corporation (SRC) Program sponsored by Defense Advanced Research Projects Agency (DARPA). The review of this letter was arranged by Editor A. Chin. *(Corresponding author: Chunlei Wu.)*

The authors are with the Department of Electrical Engineering, University of Notre Dame, Notre Dame, IN 46556 USA (e-mail: cwu10@nd.edu).

Color versions of one or more of the figures in this letter are available online at http://ieeexplore.ieee.org.

Digital Object Identifier 10.1109/LED.2020.2965330

This work is licensed under a Creative Commons Attribution 4.0 License. For more information, see http://creativecommons.org/licenses/by/4.0/

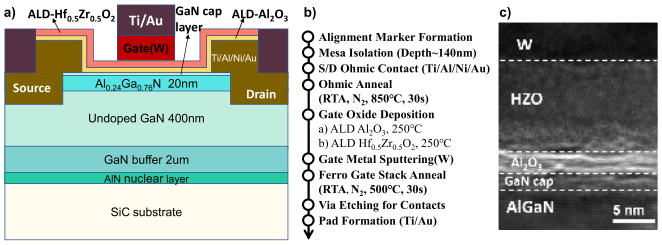

Fig. 1. (a) Schematic cross section view, and (b) Key processing steps of AlGaN/GaN FeHEMTs. (c) TEM image of the gate stack (W/ $Hf_{0.5}Zr_{0.5}O_2$/ Al_2O_3) showing the crystalline grain of HZO on AlGaN/GaN heterostructure.

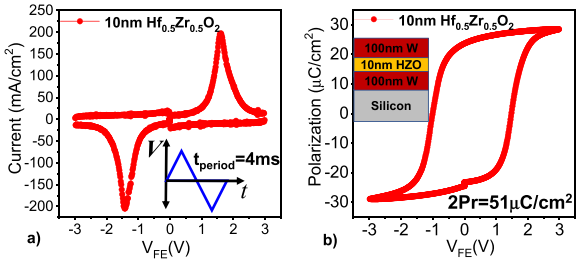

Fig. 2. (a) Measured current voltage curves of 10 nm $Hf_{0.5}Zr_{0.5}O_2$(HZO) MFM capacitor. Triangular waveforms with 4 ms period and 3 V amplitude were used. (b) PV hysteresis loop obtained, achieving 2Pr of 51 μC/cm^2. The inset shows the schematic of MFM capacitor fabricated.

ferroelectric crystallization. The FeHEMT device fabrication was completed by source/drain via etching and Ti/Au metal overlay for contacts. For all the HEMTs discussed here, the gate length is 750 nm. High resolution TEM (Fig. 1(c)) reveals the crystallinity of the ferroelectric HZO film on the AlGaN/GaN HEMT heterostructure.

III. Results and Discussion

A. Ferroelectric Gate HEMTs Characteristics

A metal-ferroelectric-metal (MFM) test structure was used to characterize the properties of the ALD-deposited HZO material. The current-voltage and P-V characteristics of a typical HZO MFM capacitor are shown in Fig. 2(a) and (b), demonstrating a remnant polarization 2Pr of 51 μC/cm^2. The ALD-grown HZO films exhibit clear ferroelectricity with FE polarization significantly larger than the total polarization of AlGaN/GaN ($\sim$2.7 μC/cm^2) [18], indicating the potential of HZO ferroelectric gate to augment polarization engineering in GaN-based HEMTs.

Fig. 3 shows the measured transfer characteristics of typical AlGaN/GaN FeHEMTs (2 nm/4 nm Al_2O_3 interlayers and 10 nm $Hf_{0.5}Zr_{0.5}O_2$) in comparison with that of a conventional AlGaN/GaN MIS-HEMT (4 nm Al_2O_3). Both forward sweep (gate voltage V_g swept from negative to positive) and backward sweep (V_g swept from positive to negative) curves are shown for a drain voltage V_d = 5 V. The transfer curves of the FeHEMTs show significant counterclockwise hysteresis, clearly indicating the FE switching of the ferroelectric gates.

A threshold voltage tuning range (ΔV_{th}) of 1.9 V has been obtained for the FeHEMT with 4 nm Al_2O_3 interlayer, while an enlarged tuning range (ΔV_{th}) of 2.8 V has been obtained for the FeHEMT with 2 nm Al_2O_3 interlayer. The increased ΔV_{th} is due to the increased MIS capacitance of the thinner Al_2O_3 layer, which enlarges the voltage drop across the ferroelectric

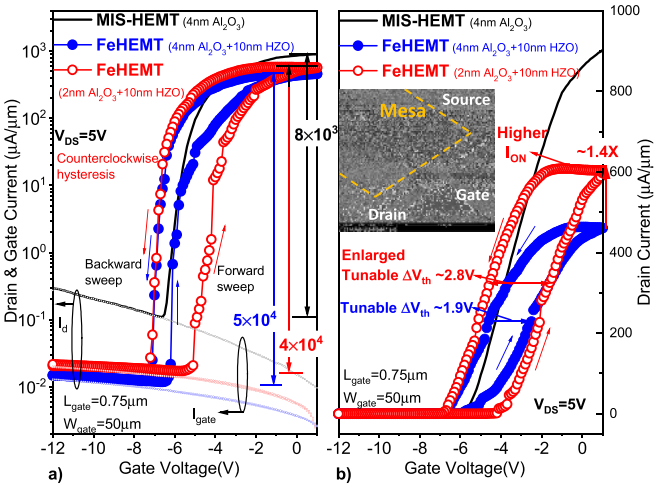

Fig. 3. Measured transfer hysteresis characteristics of AlGaN/GaN FeHEMTs in comparison with conventional MIS-HEMT in (a) semi-logarithmic and (b) linear coordinate system. FeHEMTs achieved threshold voltage tuning range (ΔV_{th}) of 1.9 V and 2.8 V for 4 and 2 nm Al_2O_3 interlayers, respectively. Inset: oblique angle SEM image of typical FeHEMT device.

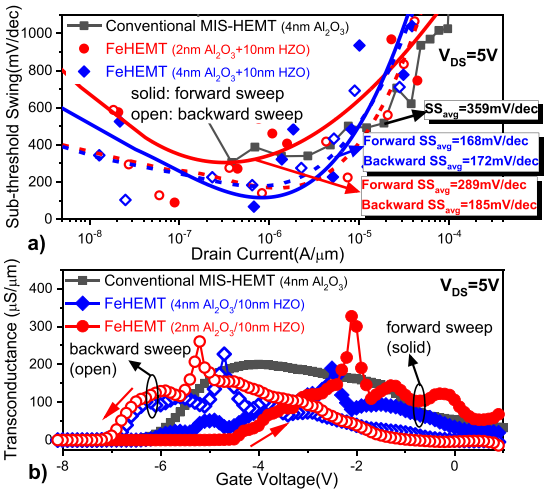

Fig. 4. (a) Measured sub-threshold swing (SS) as a function of drain current for AlGaN/GaN FeHEMTs in comparison with conventional MIS-HEMTs. (Lines: fitted to show trends). (b) Measured transconductance for AlGaN/GaN FeHEMTs in comparison with conventional MIS-HEMTs.

layer and enhances the ferroelectric polarization switching. As can be seen in Fig. 3(a), both the conventional MIS-HEMT and FeHEMTs show gate leakage limited off-currents, which is due to the mesa isolation configuration used: the FeHEMTs exhibit about one decade lower off-state leakage compared to that of the conventional MIS-HEMT, due to suppressed mesa sidewall gate leakage, which suggests the good controllability of the HZO gate stack. Additionally, the FeHEMTs show lower on-state current; this is the result of the lower MIS capacitance of the ferroelectric gate devices (due to the thicker gate stack). The 2 nm Al_2O_3 interlayer FeHEMT exhibits a 40% increase in on-state current and about 50% improvement in threshold voltage tuning range, demonstrating the benefits of the enhanced electrostatic coupling to the FE polarization.

Fig. 4(a) shows the sub-threshold swing (SS) of the FeHEMTs and the conventional MIS-HEMT. An average SS (SS_{avg}) of 172 mV/dec (for drain currents from 2×10^{-8} A/μm to 10^{-5} A/μm) is obtained in the FeHEMTs for

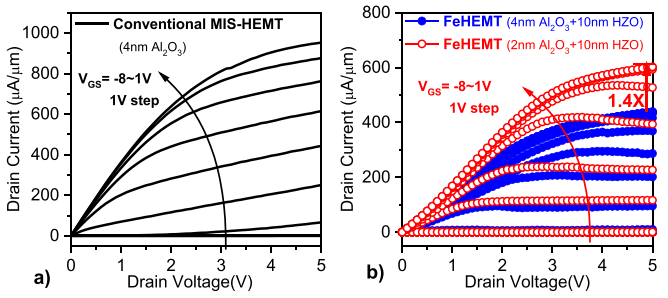

Fig. 5. (a) Measured output characteristics of conventional MIS-HEMT, and (b) FeHEMTs with Al_2O_3 thicknesses of 2 and 4 nm.

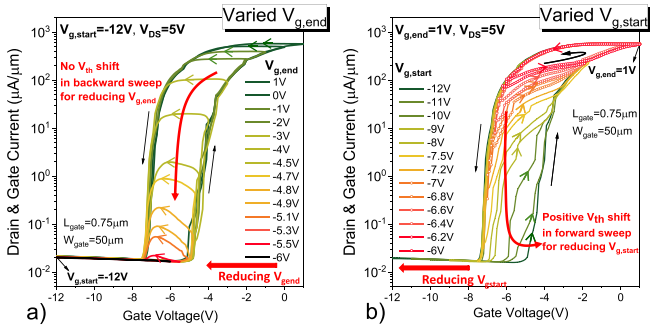

Fig. 6. (a) Measured transfer hysteresis characteristics of AlGaN/GaN FeHEMTs with varied $V_{g,end}$ from 1 V to -6 V. (b) Measured transfer hysteresis characteristics of AlGaN/GaN FeHEMTs with varied $V_{g,start}$ from -12 V to -6 V.

the backward sweeps (on-to-off sweep). This is approximately $2\times$ lower than that of the conventional MIS-HEMT (359 mV/decade, no sweep direction dependence). In FeHEMTs, when the FE polarization is switched to oppose the nitride polarization at negative gate voltage (off state), the 2DEG channel is depleted, while when the FE polarization direction is aligned with that of the nitride polarization at gate voltage above threshold (on state) [10], [11], the 2DEG concentration is increased. This enhanced abruptness of 2DEG channel modulation from the ferroelectric gate [19] leads to improved sub-threshold performance. A higher average SS was observed for forward sweeps for FeHEMTs with thinner Al_2O_3 layer, which may be due to the increased susceptibility to non-uniform FE switching from the degraded interfacial uniformity as well as higher gate fields. Both FeHEMT device types show similar SS trends in backward sweeps, which suggests that the FE dipoles are fully switchedtowards the device channel at $V_{gs} = 1V$ in both cases.

The transconductances are compared in Fig. 4(b). While the MIS-HEMT exhibits larger overall transconductance (due to its higher MIS capacitance), the FeHEMTs show distinct peaky transconductance. The relatively broad, multiple peaks in the g_m curves suggest sequential FE switching of domains [20], [21] in the gate stack along the gate width (50 μm for the devices fabricated here). Comparing the two FeHEMT structures, higher overall transconductance and peak transconductance ($g_{m,max}$) can be observed for the FeHEMT with 2nm Al_2O_3 layers, as expected from the higher MIS capacitance. In addition, on-wafer measurement indicates that the peak cutoff frequency f_t of the MIS-HEMTs is 16.5 GHz, while a typical FeHEMT has f_t of 14.9 GHz (both forward and backward gate sweeps); these are consistent with expectations for GaN HEMTs at this gate length [22], [23].

The output characteristics of both FeHEMTs and the conventional MIS-HEMT are shown in Fig. 5(a) and (b). Negative differential resistance (NDR) is evident at higher drain voltages in the FeHEMTs, which results from the FE polarization switching at the drain side of FeHEMTs. The FE domains near the drain side tend to switch back towards the device surface at higher drain voltage, leading to increasing V_{th} near the drain and the reducing drain current [24].

B. Ferroelectric Gate Stack Polarization Evaluation

The polarization switching behavior of HZO ferroelectric layer grown on AlGaN/GaN has also been evaluated. Fig. 6(a) and (b) show the dependence of the FeHEMT transfer characteristics on maximum ($V_{g,end}$) and minimum ($V_{g,start}$) gate voltages for the V_g sweep. As shown in Fig. 6(a), the transfer curves show negligible variation with reduced $V_{g,end}$ except for (as expected) a reduced maximum current. The hysteresis loop remains repeatable even for low $V_{g,end}$ around -5 V (near the turn-on voltage), indicating that the ferroelectric polarization of HZO fully switches towards the device channel (aligned with the AlGaN/GaN polarization) along with the 2DEG channel accumulation.

In contrast, the dependence of transfer curves on $V_{g,start}$ is shown in Fig. 6(b). The transfer curves show positive threshold voltage (V_{th}) shifts for more negative $V_{g,start}$. For $V_{g,start}$ less negative than -7 V, the FeHEMT reverts to conventional HEMT-like characteristic, suggesting that application of more negative gate voltages is required to fully switch the FE dipoles along the channel towards device surface (opposite to the AlGaN/GaN polarization) for 2DEG channel depletion and positive threshold voltage shifts. This clearly demonstrates the enhanced 2DEG channel modulation from ferroelectric gate in FeHEMTs. The above observations show that the FE polarization switching range of the fabricated FeHEMTs is aligned with the threshold voltage tunable range.

The FE polarization switching range of the ferroelectric gate plays crucial role in FeHEMT device performance. In order to obtain larger FE hysteresis loop as well as enhancement-mode operation for nonvolatile threshold reconfiguration, further design and process optimization of the ferroelectric gate stack and the AlGaN/GaN channel is needed.

IV. Conclusion

In this work, $Hf_{0.5}Zr_{0.5}O_2$(HZO) based ferroelectric gate HEMTs (FeHEMTs) on AlGaN/GaN heterostructures have been experimentally demonstrated. Distinct counterclockwise hysteresis has been observed in transfer characteristics in GaN based FeHEMTs. A large threshold voltage tuning range (ΔV_{th}) of 2.8 V as well as improved subthreshold performance have also been obtained due to the polarization switching of the ferroelectric gate. The results provide insights regarding the exploitation of FE gate stacks on GaN and related materials for nonvolatile RF/microwave applications.

REFERENCES

[1] T. S. Böscke, J. Müller, D. Bräuhaus, U. Schröder, and U. Böttger, "Ferroelectricity in hafnium oxide: CMOS compatible ferroelectric field effect transistors," in *IEDM Tech. Dig.*, Dec. 2011, pp. 24.5.1–24.5.4, doi: 10.1109/IEDM.2011.6131606.

[2] A. Aziz, E. T Breyer, A. Chen, X. Chen, S. Datta, S. K. Gupta, M. Hoffmann, X. Hu, A. Ionescu, M. Jerry, T. Mikolajick, H. Mulaosmanovic, K. Ni, M. Niemier, I. O'Connor, A. Saha, S. Slesazeck, S. K. Thirumala, and X. Yin, "Computing with ferroelectric FETs: Devices, models, systems, and applications," in *Proc. Design, Automat. Test Eur. Conf. Exhib. (DATE)*, Mar. 2018, pp. 1289–1298, doi: 10.23919/DATE.2018.8342213.

[3] M. Jerry, A. Aziz, K. Ni, S. Datta, S. K. Gupta, and N. Shukla, "A threshold switch augmented Hybrid-FeFET (H-FeFET) with enhanced read distinguishability and reduced programming voltage for non-volatile memory applications," in *Proc. VLSI Tech. Symp.*, Jun. 2018, pp. 129–130, doi: 10.1109/VLSIT.2018.8510679.

[4] K. Ni, J. A. Smith, B. Grisafe, T. Rakshit, B. Obradovic, J. A. Kittl, M. Rodder, and S. Datta, "SoC logic compatible multi-bit FeMFET weight cell for neuromorphic applications," in *IEDM Tech. Dig.*, Dec. 2018, pp. 13.2.1–13.2.4, doi: 10.1109/IEDM.2018.8614496.

[5] M. H. Lee, P.-G. Chen, S.-T. Fan, Y.-C. Chou, C.-Y. Kuo, C.-H. Tang, H.-H. Chen, S.-S. Gu, R.-C. Hong, Z.-Y. Wang, S.-Y. Chen, C.-Y. Liao, K.-T. Chen, S. T. Chang, M.-H. Liao, K.-S. Li, and C. W. Liu, "Ferroelectric Al: HfO_2 negative capacitance FETs," in *IEDM Tech. Dig.*, Dec. 2017, pp. 23.3.1–23.3.4, doi: 10.1109/IEDM.2017.8268445.

[6] J. Zhou, G. Han, Q. Li, Y. Peng, X. Lu, C. Zhang, J. Zhang, Q.-Q. Sun, D. W. Zhang, and Y. Hao, "Ferroelectric $HfZrO_x$ Ge and GeSn PMOSFETs with sub-60 mV/decade subthreshold swing, negligible hysteresis, and improved I_{ds}," in *IEDM Tech. Dig.*, Dec. 2016, pp. 12.2.1–12.2.4, doi: 10.1109/IEDM.2016.7838401.

[7] J. P. Ibbetson, P. T. Fini, K. D. Ness, S. P. Denbaars, J. S. Speck, and U. K. Mishra, "Polarization effects, surface states, and the source of electrons in AlGaN/GaN heterostructure field effect transistors," *Appl. Phys. Lett.*, vol. 77, no. 2, pp. 250–252, Jul. 2000, doi: 10.1063/1.126940.

[8] J. Müller, T. S. Böscke, S. Müller, E. Yurchuk, P. Polakowski, J. Paul, D. Martin, T. Schenk, K. Khullar, A. Kersch, W. Weinreich, S. Riedel, K. Seidel, A. Kumar, T. M. Arruda, S. V. Kalinin, T. Schlösser, R. B. R. van Bentum, U. Schröder, and T. Mikolajick, "Ferroelectric hafnium oxide: A CMOS-compatible and highly scalable approach to future ferroelectric memories," in *IEDM Tech. Dig.*, Dec. 2013, pp. 10.8.1–10.8.4, doi: 10.1109/IEDM.2013.6724605.

[9] J. Muüller, T. S. Boöscke, U. Schröder, S. Mueller, D. Bräuhaus, U. Boöttger, L. Frey, and T. Mikolajick, "Ferroelectricity in simple binary ZrO_2 and HfO_2," *Nano Lett.*, vol. 12, no. 8, pp. 4318–4323, Aug. 2012, doi: 10.1021/nl302049k.

[10] M. Zhang, Y. Kong, J. Zhou, F. Xue, L. Li, W. Jiang, L. Hao, W. Luo, and H. Zeng, "Polarization and interface charge coupling in ferroelectric/AlGaN/GaN heterostructure," *Appl. Phys. Lett.*, vol. 100, no. 11, Mar. 2012, Art. no. 112902, doi: 10.1063/1.3694283.

[11] Y. C. Kong, F. S. Xue, J. J. Zhou, L. Li, C. Chen, and Y. R. Li, "Ferroelectric polarization-controlled two-dimensional electron gas in ferroelectric/AlGaN/GaN heterostructure," *Appl. Phys. A, Solids Surf.*, vol. 95, no. 3, pp. 703–706, Jun. 2009, doi: 10.1007/s00339-008-4983-3.

[12] I. Stolichnov, L. Malin, P. Muralt, and N. Setter, "Ferroelectric gate for control of transport properties of two-dimensional electron gas at AlGaN/GaN heterostructures," *Appl. Phys. Lett.*, vol. 88, no. 4, Jan. 2006, Art. no. 043512, doi: 10.1063/1.2168506.

[13] L. Z. Hao, J. Zhu, Y. J. Liu, X. W. Liao, S. L. Wang, J. J. Zhou, C. Kong, H. Z. Zeng, Y. Zhang, W. L. Zhang, and Y. R. Li, "Normally-off characteristics of $LiNbO_3$/AlGaN/GaN ferroelectric field-effect transistor," *Thin Solid Films*, vol. 520, no. 19, pp. 6313–6317, Jul. 2012, doi: 10.1016/j.tsf.2012.06.040.

[14] P.-G. Chen, Y.-T. Wei, M. Tang, and M. H. Lee, "Experimental demonstration of ferroelectric gate-stack AlGaN/GaN-on-Si MOS-HEMTs with voltage amplification for power applications," *IEEE Trans. Electron Devices*, vol. 61, no. 8, pp. 3014–3017, Aug. 2014, doi: 10.1109/ted.2014.2330504.

[15] C.-T. Lee, C.-L. Yang, C.-Y. Tseng, J.-H. Chang, and R.-H. Horng, "GaN-based enhancement-mode metal–oxide–semiconductor high-electron mobility transistors using $LiNbO_3$ ferroelectric insulator on gate-recessed structure," *IEEE Trans. Electron Devices*, vol. 62, no. 8, pp. 2481–2487, Aug. 2015, doi: 10.1109/ted.2015.2446990.

[16] J. Zhu, L. Chen, J. Jiang, X. Lu, L. Yang, B. Hou, M. Liao, Y. Zhou, X. Ma, and Y. Hao, "Ferroelectric gate AlGaN/GaN E-mode HEMTs with high transport and sub-threshold performance," *IEEE Electron Device Lett.*, vol. 39, no. 1, pp. 79–82, Jan. 2018, doi: 10.1109/led.2017.2778276.

[17] L. Chen, X. Ma, J. Zhu, B. Hou, F. Song, Q. Zhu, M. Zhang, L. Yang, and Y. Hao, "Polarization engineering in PZT/AlGaN/GaN high-electron-mobility transistors," *IEEE Trans. Electron Devices*, vol. 65, no. 8, pp. 3149–3155, Aug. 2018, doi: 10.1109/TED.2018.2844335.

[18] O. Ambacher, J. Smart, J. R. Shealy, N. G. Weimann, K. Chu, M. Murphy, W. J. Schaff, L. F. Eastman, R. Dimitrov, L. Wittmer, M. Stutzmann, W. Rieger, and J. Hilsenbeck, "Two-dimensional electron gases induced by spontaneous and piezoelectric polarization charges in N-and Ga-face AlGaN/GaN heterostructures," *J. Appl. Phys.*, vol. 85, no. 6, pp. 3222–3233, Mar. 1999, doi: 10.1063/1.369664.

[19] K. Chatterjee, A. J. Rosner, and S. Salahuddin, "Intrinsic speed limit of negative capacitance transistors," *IEEE Electron Device Lett.*, vol. 38, no. 9, pp. 1328–1330, Sep. 2017, doi: 10.1109/led.2017.2731343.

[20] J. Y. Jo, H. S. Han, J.-G. Yoon, T. K. Song, S.-H. Kim, and T. W. Noh, "Domain switching kinetics in disordered ferroelectric thin films," *Phys. Rev. Lett.*, vol. 99, no. 26, pp. 267602-1–267602-4, 2007, doi: 10.1103/PhysRevLett.99.267602.

[21] H. Mulaosmanovic, J. Ocker, S. Müller, U. Schroeder, J. Müller, P. Polakowski, S. Flachowsky, R. Van Bentum, T. Mikolajick, and S. Slesazeck, "Switching kinetics in nanoscale hafnium oxide based ferroelectric field-effect transistors," *ACS Appl. Mater. Inter.*, vol. 9, no. 4, pp. 3792–3798, Feb. 2017, doi: 10.1021/acsami.6b13866.

[22] G. H. Jessen, R. C. Fitch, J. K. Gillespie, G. Via, A. Crespo, D. Langley, D. J. Denninghoff, M. Trejo, and E. R. Heller, "Short-channel effect limitations on high-frequency operation of AlGaN/GaN HEMTs for T-gate devices," *IEEE Trans. Electron Devices*, vol. 54, no. 10, pp. 2589–2597, Oct. 2007, doi: 10.1109/ted.2007.904476.

[23] S. D. Burnham, R. Bowen, J. Tai, D. Brown, R. Grabar, D. Santos, J. Magadia, I. Khalaf, and M. Micovic, "Reliability characteristics and mechanisms of HRL's T3 GaN technology," *IEEE Trans. Semicond. Manuf.*, vol. 30, no. 4, pp. 480–485, Nov. 2017, doi: 10.1109/tsm.2017.2748921.

[24] M. Jerry, J. A. Smith, K. Ni, A. Saha, S. Gupta, and S. Datta, "Insights on the DC characterization of ferroelectric field-effect-transistors," in *Proc. Device Res. Conf. (DRC)*, 2018, pp. 1–2, doi: 10.1109/DRC.2018.8442191.